N73 27414

NASA TECHNICAL MEMORANDUM

NASA TM X- 68271

NASA TM X- 68271

STUDY OF BALL BEARING TORQUE UNDER ELASTOHYDRODYNAMIC LUBRICATION

by D. P. Townsend, C. W. Allen, and E. V. Zaretsky
Lewis Research Center
Cleveland, Ohio 44135

TECHNICAL PAPER proposed for presentation at
Joint Lubrication Conference cosponsored by the
American Society of Lubrication Engineers and the
American Society of Mechanical Engineers
Atlanta, Georgia, October 16-18, 1973

STUDY OF BALL BEARING TORQUE UNDER ELASTOHYDRODYNAMIC LUBRICATION

by D. P. Townsend,* C. W. Allen,** and E. V. Zaretsky*

Lewis Research Center
National Aeronautics and Space Administration
Cleveland, Ohio 44135

ABSTRACT

Spinning and rolling torques were measured in an angular-contact ball bearing with and without a cage under several lubrication regimes in a modified NASA spinning torque apparatus. Two lubricants were used -- a di-2 ethylhexyl sebacate and a synthetic paraffinic oil, at shaft speeds of 1000, 2000, and 3000 rpm and bearing loads from 45 newtons (10 lbs) to 403 newtons (90 lbs). An analytical model was developed from previous spinning friction models to include rolling with spinning under lubrication regimes from thin film to flooded conditions. The bearing torque values have a wide variation, under any condition of speed and load, depending on the amount of lubricant present in the bearing. The analytical model compared favorably with experimental results under several lubrication regimes.

E-7284

---

*NASA-Lewis Research Center, Member ASME.
**University of California, Chico, Member ASME.

NOMENCLATURE

A_c	area of cage land, m^2 ($in.^2$)
a	major semiaxis of contact ellipse, m (in.)
b	minor semiaxis of contact ellipse, m (in.)
b'	semiwidth of contact ellipse at y, m (in.)
C	radial cage clearance, m (in.)
C_D	drag coefficient
E	materials properties factor, N/m^2 (psi)
$E_{1,2}$	modulus of elasticity, N/m^2 (psi)
e	exponent
$\hat{e}$	unit vector along bearing axis
F	lubricant factor
F_c	cage force, N (lb)
F_D	fluid-dynamic drag, N (lb)
F_H	friction force due to hysteresis, N (lb)
F_R	friction force due to rolling drag, N (lb)
F_S	friction force due to microslip, N (lb)
f	coefficient of friction
h	film thickness, m (in.)
h_o	minimum distance between ball and groove, m (in.)
$\hat{i},\hat{j},\hat{k}$	unit vector in x, y, and z direction
K	constant defining outer boundary of integration
M_s	total spinning torque at ball/race interface, N-m (lb-in.)
M_{s1}	total spinning torque in Hertzian ellipse, N-m (lb-in.)
M_{s2}	spinning torque due to viscous drag outside Hertzian ellipse, N-m (lb-in.)

N	number of balls
P	normal load, N (lb)
R	radius of ball, m (in.)
R_e	radius of equivalent cylinder, m (in.)
R_G	radius of groove, m (in.)
R_L	cage land radius, m (in.)
R_p	pitch radius, m (in.)
R_R	radius of race, m (in.)
r	polar coordinate, m (in.)
r_o	value of r at outer boundary of Hertzian ellipse, m (in.)
S	contact stress, N/m^2 (psi)
T	total bearing torque, N-m (lb-in.)
T_c	cage torque, N-m (lb-in.)
T_1	bearing torque due to ball spin torque, N-m (lb-in.)
T_2	bearing torque due to rolling drag, N-m (lb-in.)
T_3	bearing torque due to aerodynamic drag, N-m (lb-in.)
T_4	torque due to hysteresis, N-m (lb-in.)
T_5	bearing torque due to cage drag, N-m (lb-in.)
U_B	surface velocity of ball relative to moving coordinate system, m/sec (in./sec)
U_c	linear velocity of ball center, m/sec (in./sec)
U_R	surface velocity of race relative to moving coordinate system, m/sec (in./sec)
U_S	relative slip velocity between ball and race, m/sec (in./sec)
W	load per unit width, N/m (lb/in.)
x, y, z	moving coordinate system, m (in.)
α	pressure-viscosity exponent, $(N/m^2)^{-1}$ (psi^{-1})

β angle which ball angular velocity vector makes with bearing axis, deg

θ loaded contact angle, deg

μ absolute viscosity, N-sec/m^2 (lb-sec/in.^{2})

μ_o ambient viscosity, N-sec/m^2 (lb-sec/in.^{2})

ν Poisson's ratio

ρ density of fluid, kg/m^3 (lb-sec^2/in.^{4})

τ shear stress, N/m^2 (psi)

τ_c transition shear stress, N/m^2 (psi)

ϕ polar coordinate in the x-y plane

Ω_c angular velocity of ball center, rad/sec

Ω_i angular velocity of inner race, rad/sec

Ω_o angular velocity of outer race, rad/sec

ω angular velocity of ball with respect to rotating coordinate system, rad/sec

ω_i relative angular velocity of inner race with respect to moving coordinate system, rad/sec

ω_o relative angular velocity of outer race with respect to moving coordinate system, rad/sec

ω_r angular velocity of rolling, rad/sec

ω_s angular velocity of spinning, rad/sec

Subscripts:

i denotes inner race

o denotes outer race

$\rightarrow$ indicates vectors

INTRODUCTION

In bearing and gear applications considerable power losses can occur even when good lubrication is present. In rolling-element bearings

these power losses result in heat generation and increased temperature of the lubricant and the bearing components. These losses occur due to a number of factors; shearing of the lubricant in the bearing cavities, rubbing of the balls and cage (separator), cage drag, spinning and rolling of the balls in the raceways and churning of the lubricant. Ball bearing kinematics are also affected by these losses. Early analytical work [1-3][1] on power losses in ball bearings were restricted to the use of Coulomb friction at the sliding contacts. More recently it has become evident that the Coulomb friction model is inadequate to completely describe all the conditions in a real bearing [4, 5]. In the later analysis [5] the EHD lubricant film and the rheological properties of the lubricant were used to determine bearing friction and kinematics. The method of [5] uses an exponential model for the lubricant pressure-viscosity characteristics which may predict power losses higher than those which generally occur in practice.

The torque of a ball spinning in a groove with different conformities and several lubricants was measured [6-8] in the NASA spinning torque apparatus. Later, an analytical model was developed [9, 10] which predicted the extent that elastohydrodynamic film contributed to the effective ball/race separation and spinning torque. The analyses showed that conventional elastohydrodynamic lubrication is possible in the case of a groove having conformities up to 60 percent.

In developing the analysis of [9] it was found that the assumption of a Newtonion fluid with an exponential pressure-viscosity relationship gave

---

[1] Numbers in brackets designate references at end of paper.

impossibly high values of torque. It was necessary therefore to introduce a cutoff point at which the pressure-viscosity exponent decreased to a much lower value. The model of [9] yielded satisfactory results when the calculated shear rate was of the order of 10^6 reciprocal seconds. Comparison with data of other researchers [11] showed the cutoff to occur at much higher pressures when the film thicknesses were much greater than those of [9]. In other words, a lower shear rate resulted in a higher cutoff pressure.

The research reported herein, which is based on the work reported initially in [12, 13], was undertaken to investigate the losses which occur in an angular-contact ball bearing under spinning and rolling motion of the balls. The objectives were: (a) Modify the composite viscosity lubricant model to take into account the shear rate dependency effects; (b) Measure experimentally the torque in a thrust-loaded ball bearing with and without a cage; (c) Extend the previously-developed analytical techniques for determining torque of a ball spinning in a nonconforming groove to the case of a bearing operating with combined spinning and rolling; and (d) Determine analytically the effect of lubricant viscosity and fluid-dynamic drag on bearing torque.

APPARATUS, SPECIMENS, AND PROCEDURE

Spinning Torque Apparatus

A spinning torque apparatus (see figs. 1(a) and (b)) described previously in [6, 7] was also used for the tests reported herein. The apparatus essentially consists of a turbine drive, a pneumatic load device, an upper and lower test specimen, a lower test-housing assembly incorporating a

hydrostatic airbearing, and a torque-measuring system. An angular-contact ball bearing can be substituted for the upper and lower test specimen in the apparatus. In operation, the bearing inner race is pneumatically loaded against the balls of the bearing through the drive shaft. As the drive shaft is rotated, the inner race rotates with respect to the outer race in the bearing. This causes an angular deflection of the outer race housing. This angular movement is sensed optically by the torque-measuring system and is converted into a torque value. During a test, the torque is continuously recorded on a strip chart.

Test Bearings

Two types of test bearings were used. Both types were conventional 204-size angular-contact bearings with all but three balls removed. One bearing had a 26° contact angle with a 52-percent conformity at inner and outer races. The second bearing had a 17° contact angle with 53- and 54-percent conformity at the inner and outer races, respectively. Specifications of the bearings are given in Table 1.

Test Procedure

Tests were conducted in the spinning torque apparatus at room temperature using the two test bearings both with and without a cage. Test conditions were 1000, 2000, and 3000 rpm and varying loads from 44.5 N (10 lb) to 403 N (90 lb). The tests were conducted with two lubricants, a di-2-ethylhexyl sebacate and a synthetic paraffinic oil.

The bearings were first run without a cage and using oil jet lubrication at a rate of 8 cc/min. After the initial tests the bearing was

cleaned and a few drops of lubricant which had been diluted by a 5 to 1 addition of hexane was applied. The hexane then evaporated leaving only a thin film of lubricant on the bearing surfaces. The bearings were then run again but only long enough (usually 5 to 15 sec) at each speed and load condition to reach equilibrium conditions. Finally, the bearings were run with an inner-race riding cage with jet lubrication.

ANALYSIS

Generalized Rheological Model

The composite viscosity lubricant model [9] was modified to take into account the shear rate dependency effects of a lubricant [12]. The new rheological model incorporates four parameters: (a) Ambient viscosity μ_o, (b) Pressure-viscosity coefficient α, (c) a lubricant factor F, and (d) transition shear stress, τ_c. These parameters may be represented by the following relations

$$\tau = \mu_o e^{\alpha S} \omega y/h \quad \text{and} \quad \tau < \tau_c \tag{1a}$$

$$\tau = \mu_o e^{\alpha S} \omega y/h \quad \text{and} \quad \tau_c < \tau < FS \tag{1b}$$

$$\tau = FS \quad \text{and} \quad \mu_o e^{\alpha S} \omega y/h > FS \tag{1c}$$

The transition shear stress τ_c is introduced to allow for large ratios τ/S to be present when the pressure is low. The introduction of a lubricant factor, F serves to limit the shear stress at high pressures and shear rates to a fraction of the normal stress. In order to visualize the behavior of the fluid under the foregoing conditions, Fig. 2 shows a plot of shear

stress as a function of normal stress for a synthetic paraffinic lubricant at various shear rates. If the shear stresses computed by Eqs. (1a), (1b), or (1c) are substituted into the equation for shear stress, where $\tau = \mu \frac{\omega y}{h}$, an equivalent viscosity may be obtained for any shear rate. Fig. 3 shows this equivalent viscosity for various shear rates with the new model and also for the composite viscosity lubricant model of [9]. The previous model is seen to be approximately equivalent to a special case of the newer, more general, model.

The spinning moments for a synthetic paraffinic lubricant were computed using the revised rheological model and were compared with the experimental values from [8]. The theoretical results showed good agreement with the experimental data of [8]. The parameters used in the rheological model for the synthetic paraffinic lubricant were determined to be:

$\mu_o = 0.414$ N-sec/m^2 (6×10^{-5} lb-sec/in.^{2})

$\alpha = 1.33\times10^{-8}$ m^2/N (0.92×10^{-4} psi^{-1})

$\tau_c = 6.89\times10^6$ N/m^2 (1000 psi)

$F = 0.07$

For the di-2-ethylhexyl sebacate lubricant tests which were reported in [3] the following fluid parameters were determined:

$\mu_o = 0.016$ N-sec/m^2 (0.24×10^{-5} lb-sec/in.^{2})

$\alpha = 1.45\times10^{-8}$ m^2/N (1.0×10^{-4} psi^{-1})

$\tau_c = 6.89\times10^6$ N/m^2 (1000 psi)

$F = 0.045$

The synthetic paraffinic oil and the di-2-ethylhexyl sebacate were the same fluids used for the testing reported herein. The above lubricant

properties and generalized model were used in the analysis presented in this paper.

Origin of Friction Torque

In a lubricated ball bearing there is an elastohydrodynamic film between each race and ball. There is also some lubricant surrounding the high-pressure elastohydrodynamic region. Among the possible sources of bearing friction in a thrust bearing of the type under investigation, are the following:

1. Spinning friction arising within the elastohydrodynamic region.
2. Spinning friction due to the lubricant outside of this region.
3. Rolling resistance due to the lubricant being squeezed out in front of the rolling ball.
4. Friction due to translational sliding in the elastohydrodynamic region.
5. Fluid-dynamic drag of the balls as they orbit about the center of the bearing.
6. Hysteresis losses due to elastic deformation of steel during rolling.
7. Cage viscous drag.

The contribution to the bearing torque of each of these effects will be considered independently and then the total bearing torque obtained by the summation of the individual contributions. For the first order computation, coupling between the various effects will be neglected.

Spinning Torque

Analysis of the spinning torque is an extension of the work undertaken previously for the spinning of a ball in a nonconforming groove [9, 10].

The coordinate system for a ball bearing system is shown in Fig. 4. The contact ellipse for the ball/race interface is shown in Fig. 4(b). As in the case of the pure spinning reported in [9, 10] several simplifying assumptions are made as follows:

(a) The stress distribution is Hertzian.

(b) The major axis of the ellipse is assumed to be considerably greater than the minor axis. For a 54 percent curvature, the ratio of the major to minor axis is 5.2. For curvature less than 54 percent this ratio is larger.

(c) The major axis of the contact ellipse is considerably less than the ball radius so that the ellipse may be approximated by a plane ellipse lying in the x-y plane.

(d) The significant velocities, as far as film thickness and torque are concerned, are those in the x direction. This follows from the second assumption.

(e) The nonsymmetry of the film thickness in the positive and negative y directions is assumed to be small so that moments can be assumed to be balanced about the z axis.

(f) The surface roughness is assumed small in comparison with the thickness of the elastohydrodynamic film.

(g) Frictional resistance is entirely due to viscous shear.

(h) Side leakage is neglected.

(i) The film thickness in the x direction is constant.

(j) The surfaces are isothermal.

On the basis of the preceding assumptions, the system can be reduced

to a number of elemental rollers of width dy in rolling and sliding motion relative to the groove (Fig. 4).

The equation for the resulting spin torque about the z axis is derived in Appendix I by integrating the elemental moments over the whole contact ellipse as:

$$\overrightarrow{M_{s1}} = \int d\overrightarrow{M_{s1}} = \int y\hat{j}\, \overrightarrow{dF} \tag{3}$$

In addition to the effect on spinning torque of the lubricant within the Hertzian contact region, the effect of the lubricant outside of this region must also be considered. The expression for this moment is given in [8]

$$M_{s2} = 4\mu\omega_s \int_0^{\pi/2} \int_{r_0}^{KR} \frac{r^3\, d\phi\, dr}{\left(R + h - \frac{R_G}{\cos\phi}\right) + \left[\left(\frac{R_G}{\cos\phi}\right)^2 - r^2\right]^{1/2} - (R^2 - r^2)^{1/2}} \tag{4}$$

This may be integrated numerically over the region outside the contact ellipse. The total moment M_s, is therefore the sum of the moments given by the Eqs. (3) and (4)

$$M_s = M_{s1} + M_{s2} \tag{5a}$$

Spinning torques are computed for both inner and outer ball/race contacts. For equilibrium it is necessary for the net moment vector on the ball in the z direction to be zero. Therefore,

$$\overrightarrow{M_{si}} + \overrightarrow{M_{so}} = 0 \tag{5b}$$

The values of the spinning torque at the inner and outer ball/race contacts are dependent upon the relative spin velocities which are in turn dependent upon the angle β of the angular velocity vector. In order to obtain the correct value of β, two extreme values are assumed and the net moment on the ball computed for each and an interpolation procedure is used to arrive at that value for which the net moment on the ball is close to zero. The criterion used in the numerical computation is

$$\frac{\left|\vec{M}_{si} + \vec{M}_{so}\right|}{\left|\vec{M}_{si}\right| + \left|\vec{M}_{so}\right|} < 0.01 \tag{6}$$

When the net moment has been obtained within the limit defined by Eq. (6), the resulting bearing torque due to ball spinning friction only is obtained as:

$$T_1 = NM_s \sin \theta \tag{7}$$

The above analysis does not take into consideration the effect of centrifugal force at high speed.

Rolling Resistance

As the ball rolls in the groove, lubricant is squeezed out ahead of the ball/race contact as shown in Fig. 5(a). However, if inertia effects are neglected, the ball must be in equilibrium. Therefore, some microslip must be present in order to provide balancing forces F_{Si} and F_{So} (Fig. 5(c)).

A simple force analysis shows that for equilibrium:

$$F_{Si} - F_{So} - F_{Ri} + F_{Ro} = 0 \tag{8}$$

and by taking moments about the center of the ball

$$R(F_{Si} - F_{Ri}) + R(F_{So} - F_{Ro}) = 0 \tag{9a}$$

It may be seen that

$$F_{Si} = F_{Ri} \tag{9b}$$

$$F_{So} = F_{Ro} \tag{9c}$$

The rolling velocities are obtained from the kinematics outlined from [4]. The shear force due to rolling is obtainable from the analysis presented in [14] and modified for a ball-race contact [13].

The torque on the inner ring due to the rolling resistance is then given by

$$T_{2i} = 2F_{Ri}\, NR_{Ri} \tag{10a}$$

Similarly the torque on the outer ring is given by

$$T_{2o} = 2F_{Ro}\, NR_{Ro} \tag{10b}$$

The preceding analysis is based upon the assumption that the microslip necessary to provide the forces F_{Si} and F_{So} is small in comparison with the other motion of the ball/race system and therefore does not significantly change the kinematics of the bearing.

Fluid Dynamic Drag

As the balls orbit within the bearing there is a drag force present which is approximately equivalent to the drag of a sphere submerged in a fluid. An approximate analysis of this can be made using the following assumptions:

1. Each ball is assumed to behave as it would while moving in a steady stream of fluid.

2. Interaction of the balls with each other is neglected.

3. Any effect due to rotation of the balls is neglected.

On the basis of the preceding assumptions the drag F_D of a single ball may be computed by the following formula [15].

$$F_D = C_D \pi R^2 (1/2\rho U_c^2) \tag{11}$$

A difficulty arises because the density of the medium must be known. The viscosity of the medium also must be known because the drag coefficient C_D is dependent upon the Reynolds number [15]. The annular space, however, is not filled with a homogeneous fluid but a mixture of air and lubricant.

The drag force may, however, be bracketed by computing one value based upon air alone and another value based on the annular space being filled with lubricant.

As shown in Fig. 6, for equilibrium the drag force must be balanced by forces at the inner and outer ball/race contact. These forces would be caused by microslip at the ball/race contact and would each be equal to

$F_D/2$. The resulting torque on the inner race is then:

$$T_{3i} = R_{Ri}\, F_D/2 \tag{12a}$$

and on the outer race is

$$T_{3o} = R_{Ro}\, F_D/2 \tag{12b}$$

The torque at the inner race therefore adds to the friction torque seen by the rotating inner ring. The fluid drag torque on the outer race acts in the opposite direction to the other torque values previously discussed (see Fig. 6). Hence, the value of fluid drag torque should be subtracted from the other torque values previously discussed.

Hysteresis

When a ball rolls on a plate or in a groove, elastic deformation of the ball and groove will occur. The application and relaxation of load as the ball rolls along the groove will result in a certain amount of hysteresis loss within the stressed zones of the ball and groove.

An experimental investigation of the hysteresis loss for balls rolling on a flat plate was reported in [16]. A semi-analytical relationship was derived in [16] between the specific damping capacity of the material and the resisting force. This relationship is:

$$F_H = 0.1315 \left(\frac{1}{E_1} + \frac{1}{E_2}\right)\left(\frac{P}{a}\right)^2 \times \text{Specific damping capacity} \tag{13}$$

For an AISI 52100 steel ball (R_c60) a value of the specific damping capacity of 0.007 is given in [16].

Since the stressed region is assumed to be that enclosed within the Hertzian contact region, Eq. (13) may be modified for an elliptic contact region similar to that present between a ball and groove by substituting the area of an ellipse for that of a circle. Equation (13) then becomes

$$F_H = 0.1315\left(\frac{1}{E_1} + \frac{1}{E_2}\right)\left(\frac{P^2}{ab}\right) \times \text{Specific damping capacity} \qquad (14)$$

The torque on the outer race due to hysteresis is then obtained as:

$$T_{4o} = NF_H (R_p + R \cos \theta) \qquad (15)$$

Cage Drag

Reference is made to Fig. 7, which is a diagram of an inner race riding cage with radial clearance C and a nominal rubbing area A_c. If it is assumed that (a) the radial clearance C is constant and is much less than the land radius R_L; (b) the region between the cage and land is filled with lubricant; and (c) the velocity gradient in the radial direction is linear, the Pretroff formula for drag of a concentric plane bearing may be used to determine cage drag.

On the basis of the foregoing assumptions the shear stress within the lubricant is given by

$$\tau = \mu \frac{(\Omega_c - \Omega_i) R_L}{C} \qquad (16)$$

The total cage torque would be given by:

$$T_c = \mu (\Omega_c - \Omega_i) A_c R_L^2 / C \qquad (17)$$

In order to consider the effect of this on the overall bearing torque, the bearing ball cage system shown in Fig. 7 must be considered. If inertia forces are neglected and the friction between the ball and cage is also neglected, then for equilibrium

$$\text{Ball/cage reaction} = \frac{T_c}{R_p} \tag{18a}$$

$$\text{Race/ball reaction} = \frac{T_c}{2R_p} \tag{18b}$$

The torque on the outer race induced by the cage is

$$T_{5o} = \frac{T_c R_{Ro}}{2R_p} \tag{19}$$

The preceding analysis considers the kinematic conditions to remain the same as for the cageless bearing. Also, the friction between ball and pocket is neglected. By considering the equilibrium of the ball as shown in Fig. 7(c) with a constant coefficient of friction f,

$$F_{co} = \frac{F_c}{2}(1 + f) \tag{20}$$

The torque on the outer race due to the cage is therefore increased by a factor of $(1 + f)$. For an effective coefficient of friction, $f = 0.2$ the effect would be a 20 percent increase in the torque due to the cage.

Total Bearing Torque

Neglecting coupling between the various effects considered individually, and combining Eqs. (7), (10b), (12b), (15) and (19), the gross torque on the outer race can be obtained where

$$T = T_{1o} + T_{2o} - T_{3o} + T_{4o} + T_{5o} \tag{21}$$

RESULTS AND DISCUSSION

The bearing total friction torques were measured experimentally for all specimen and lubricant combinations at loads varying from 44.5 newtons (10 lb) to 403 newtons (90 lbs) and for speeds of 1000, 2000, and 3000 rpm. For each lubricant, the torque was measured under conditions of a full supply of lubricant to the bearing and then with a thin film of lubricant only.

Experimental torque results for the di-2-ethylhexyl sebacate for the 17^{o} and 26^{o} contact angle bearing are shown in Fig. 8 for oil-jet lubrication. The same tests were repeated for thin-film lubrication. However, no significant difference was found between the experimental results for the full lubrication condition and the thin film case. The analytical values for the outer races are also shown in Fig. 8. Calculated values for the fluid-dynamic drag have not been included because of the unknown nature of the fluid within the annular region.

The experimental torque values with the synthetic paraffinic oil lubricant with oil jet lubrication for the bearings without a cage and with the 17^{o} and 26^{o} contact angles are shown in Fig. 9. The calculated values for the combined spinning and rolling torque are shown in the same figures. There is fair agreement between experimental and analytical values of

torque for oil jet lubrication. The calculated values of torque increase more with speed than do the experimental values. This result is most likely caused by more lubricant being centrifugally thrown out of the bearing as the speed increases for the experimental values.

The experimental results for the thin film lubrication with the synthetic paraffinic oil are shown in Fig. 10. From these data it is seen that the speed effect is practically nonexistent for the conditions shown. The experimental trend of the data agree closely with the calculated values of torque considering the spinning term (eq. (7)) and hysteresis loss (eq. (15)) only.

Using the synthetic paraffinic lubricant, the bearing torque with jet lubrication was an order of magnitude greater than the torque with thin film lubrication (Figs. 9 and 10). However, using the di-2-ethylhexyl sebacate lubricant, the bearing torque was essentially the same with both jet and thin film lubrication. This is because the di-2-ethylhexyl sebacate is much less viscous than the synthetic paraffinic oil and was not fully retained in the bearing with jet lubrication.

The computed minimum and maximum torques expected from the fluid-dynamic drag are given in Table 2. The minimum value is determined by considering the annular space in the bearing to be filled with air only. To determine the maximum value of fluid-dynamic drag, the annular space is considered to be completely filled with lubricant. On the basis of air alone, the contribution of fluid-dynamic drag to the total bearing torque is insignificant. If it is assumed that the annular space is completely filled with the synthetic paraffinic oil, a maximum value of fluid-dynamic torque of 8.6×10^{-3} newton-meters (0.076 lb-in.) at 3000 rpm is calculated.

The computed bearing torques due to hysteresis effects only, are shown in Fig. 11. These torques are dependent only upon load and contact angle and are independent of speed and lubricant. However, the hysteresis effect alone is insignificant when compared with the other factors considered.

The agreement between the experimental results and computed values for the bearings without a cage is generally good, although the computed torque is, with few exceptions, less than the corresponding experimental value. In all cases, an extrapolation of the curves back to the zero load point yields a finite torque at the no-load condition. This is to be expected in the case of the di-2-ethylhexyl sebacate and the synthetic paraffinic lubricants with adequate lubricant supply because the rolling resistance through the lubricant will still be present with zero load. However, for the case of the thin film, the only torques computed are those due to the ball spin and hysteresis effects. There would, however, be a small torque due to rolling resistance with any nonzero lubricant film. Addition of the torque would raise the computed value by approximately the same amount over the whole load range, and bring the computed and experimental values into closer agreement.

The experimental and calculated bearing torques which include cage drag are shown in Figs. 12. Figures 12(a) and (b) show the results for the two bearings with the di-2-ethylhexyl sebacate lubricant. With this lubricant, the calculated and experimental torques are in fair agreement. Comparing Figs. 12(a) and (b) with Figs. 8(a) and (b), respectively, the calculated values of cage drag were found to account for approximately

98 percent of the total bearing torque at a thrust load of 44.5 newtons (10 lb) and approximately 93 percent at a thrust load of 403 newtons (90 lb) and a speed of 3000 rpm for the bearing with the 26^{o} contact angle. For the bearing with the 17^{o} contact angle under the same conditions, cage drag accounted for approximately 97 and 92 percent of the total calculated bearing torque, respectively. The experimental values of cage drag were found to be approximately 95 and 87 percent, respectively, for the bearing with the 20^{o} contact angle. For the bearing with the 17^{o} contact angle, the experimental values of cage drag were approximately 95 and 85 percent, respectively, of the entire bearing torque under the same experimental conditions.

Figure 12(c) and (d) are the results for the two bearings with the synthetic paraffinic oil lubricant. It is apparent that except at the speed of 1000 rpm, the calculated torques are as much as approximately 100 percent greater than the experimental values. The most probable reason for this discrepancy at the higher speeds is that the more viscous synthetic paraffinic oil does not completely fill the bearing cavity but is either centrifuged out of the bearing or may not enter the cage-land area of the inner race in large quantities. As a result, less torque would occur than calculated.

Comparing the torque data of Figs. 12(c) and (d) with Figs. 9(a) and (b) for the synthetic paraffinic oil, the calculated values of cage drag at a speed of 3000 rpm and a thrust load of 403 newtons (90 lbs) were approximately 27 and 29 percent of the total calculated bearing torque for the 17^{o} and 20^{o} contact angle bearing, respectively. Under the same conditions, the experimental values of cage torque were approximately 2 and 10 percent, respectively, of the total experimental bearing torque.

These results would clearly indicate that with a viscous fluid, such as the synthetic paraffinic oil, cage drag is less of a factor in total torque values than with a less viscous fluid, such as the di-2-ethylhexyl sebacate. Further, these results would tend to affirm the previous speculation that the lubricant dues not enter the cage-land area of the inner race in large quantities with the viscous lubricant.

SUMMARY

The Spinning Torque Apparatus was modified to measure the torque on a thrust loaded 204 size (20-mm bore) ball bearings having contact angles of 17^{o} and 26^{o} with and without a cage. Friction torque was measured for thrust loads varying from 44.5 newtons (10 lbs) to 403 newtons (90 lbs) at speeds of 1000, 2000, and 3000 rpm. Tests were conducted with either a di-2-ethylhexyl sebacate and a synthetic paraffinic oil as the lubricant. The lubrication mode was either oil jet lubrication directed at the bearing contacting surfaces of a thin surface film of lubricant applied on the bearing races and balls. An analytical model which included rolling resistance and a generalized rheological model was developed and extended from previous model for spinning torque and lubricant rheology. The following results were obtained:

1. The calculated bearing torques using the bearing analytical model and lubricant rheological model developed for determining the torques in a thrust-loaded ball bearing were in fair agreement with the experimental results.

2. Cage drag was found to be primarily a function of lubricant viscosity.

For the di-2-ethylhexyl sebacate, cage drag was found to account for approximately 87 to 95 percent of total experimental bearing torque. However, for the more viscous synthetic paraffinic oil, cage drag was found to account for approximately 2 to 10 percent of total experimental bearing torque.

3. For a bearing without a cage with a relatively low viscosity fluid such as the di-2-ethylhexyl sebacate the largest contribution to bearing torque was ball spin torque. For a more viscous oil such as the synthetic paraffinic oil, the largest contributor to bearing torque is the resistance to rolling through the lubricant. The resistance to rolling is affected by the amount of lubricant present.

4. With a low viscosity lubricant an excess supply of lubricant to the bearing has a small affect on bearing torque. However, with a viscous lubricant, a nominal flow of oil to the bearing can result in a tenfold increase in bearing torque when compared with the value obtained with only a thin film of lubricant present.

APPENDIX

Derivation of Spinning Torque

Analysis of the spinning torque is an extension of the work undertaken previously for the spinning of a ball in a nonconforming groove [9, 10]. The contact ellipse for the ball/race interface is shown in Fig. 4. The system can be reduced to a number of elemental rollers of width dy in rolling and sliding motion relative to the groove (Fig. 4). Relative to the rotating coordinate system the surface velocity of the elemental roller is obtained from [13] for the inner race as:

$$U_{Bi} = -(\omega_{ri} R + \omega_{si} y) \tag{A1a}$$

and for the outer race as:

$$U_{Bo} = (\omega_{ro} R - \omega_{so} y) \tag{A1b}$$

The magnitude of the surface velocities of the inner and outer races with respect to the rotating coordinate systems are:

$$U_{Ri} = \omega_{ri} R \tag{A2a}$$

$$U_{Ro} = \omega_{ro} R \tag{A2b}$$

The slip velocity of the ball with respect to the inner race from [13] is obtained as:

$$U_{Si} = -\omega_{si} y \tag{A2c}$$

and for the outer race

$$U_{So} = -\omega_{so} y \tag{A2d}$$

The tractive force on each element of the contact ellipse is then given as:

$$\vec{dF} = \int_{-b'}^{b'} \tau dx\, dy\, \hat{i} \tag{A3}$$

For a Newtonian fluid with a linear velocity gradient

$$\tau = \mu U_S / h \tag{A4}$$

where the film thickness h is given in [17] as

$$h = \left(\frac{1.6\ \alpha^{0.6}\ E^{0.03}\ R_e^{0.43}\ \mu_o^{0.7}}{W^{0.13}} \right) \left(\frac{U_B + U_R}{2} \right)^{0.7} \tag{A5a}$$

and

$$E = \frac{2}{\frac{1 - \nu_1^2}{E_1} + \frac{1 - \nu_2^2}{E_2}} \tag{A5b}$$

$$R_e = \frac{RR_R}{R + R_R} \tag{A5c}$$

$$W = \frac{0.75P}{a} \left[1 - \left(\frac{y}{a} \right)^2 \right] \tag{A5d}$$

According to [12] the assumption of Newtonian behavior for the lubricant is not realistic at high pressures and shear rates and a more general model is:

$$\tau = \mu_o e^{\alpha S} U_S/h \quad \text{and} \quad \tau < \tau_c \tag{A6a}$$

$$\tau = \mu_o e^{\alpha S} U_S/h \quad \text{and} \quad \tau_c < \tau < FS \tag{A6b}$$

$$\tau = FS \quad \text{and} \quad \mu_o e^{\alpha S} U_S/h > FS \tag{A6c}$$

The resulting spin torque about the z axis is then obtained by integrating the elemental moments over the whole contact ellipse as:

$$\vec{M}_{s1} = \int d\vec{M}_{s1} = \int y\hat{j}\, d\vec{F} \tag{A7}$$

The computation of the shear stress τ proceeds as follows

1. At a given value of y the film thickness is computed using Eq. (A5a).

2. For each value of x at the given value of y the Hertzian contact pressure is given by

$$S = \frac{1.5P}{\pi ab}\left[1 - \left(\frac{y}{a}\right)^2 - \left(\frac{x}{b}\right)^2\right]^{1/2} \tag{A8}$$

3. The shear stress τ is computed by Eq. (A6a) if its value is less than the critical shear stress τ_c. If the shear stress is larger than τ_c but less than FS it is computed by Eq. (A6b). However, if the shear stress is larger than FS, Eq. (A6c) is used.

REFERENCES

1. Poritsky, H. Hewlett, C. W., Jr. and Coleman, R. E., Jr. "Sliding Friction of Ball Bearings of the Pivot Type," J. Appl. Mech., Vol. 14, No. 4, Dec. 1947, pp. 261-268.

2. Jones, A. B. "Ball Motion and Sliding Friction in Ball Bearings," J. Basic Eng., Vol. 81, No. 1, Mar. 1959, pp. 1-12.

3. Reichenbach, G. S., "The Importance of Spinning Friction in Thrust-Carrying Ball Bearings," J. Basic Eng., Vol. 82, No. 2, June 1960, pp. 295-301.

4. Harris, T. A., "Ball Motion in Thrust-Loaded Angular Contact Bearings with Coulomb Friction," J. Lub. Tech. Vol. 93, No. 1, Jan. 1971, pp. 32-38.

5. Harris, T. A., "An Analytical Method to Prevent Skidding in Thrust-Loaded Angular Contact Ball Bearings," J. Lub. Tech., Vol. 93, No. 1, Jan. 1971, pp. 17-24.

6. Miller, T., Parker, J., and Zaretsky, E. V., "Apparatus for Studying Ball Spinning Friction," NASA TN D-2796, 1965.

7. Dietrich, M. W., Parker, R. J., and Zaretsky, E. V., "Effect of Ball-Race Conformity on Spinning Friction." NASA TN D-4669, 1968.

8. Dietrich, M. W., Parker, R. J., Zaretsky, E. V., and Anderson, W. J , "Contact Conformity Effects on Spinning Torque and Friction," J. Lubr. Tech., Vol. 91, No. 2, Apr. 1969, pp. 308-313.

9. Allen, C. W., Townsend, D. P., and Zaretsky, E. V., "Elastohydrodynamic Lubrication of a Spinning Ball in a Nonconforming Groove," J. Lubr. Tech., Vol. 92, No. 1, Jan. 1970, pp. 89-96.

10. Allen, C. W., Townsend, D. P., and Zaretsky, E. V., "Comparison of Conventional and Microasperity Elastohydrodynamic Lubrication of a Ball Spinning in a Nonconforming Groobe," NASA TN D-6761, April 1972.

11. Johnson, K. L., and Cameron, R., "Shear Behaviour of Elastohydrodynamic Oil Films at High Rolling Contact Pressures," Proc. Inst. Mech. Eng., Vol. 182, No. 14, 1967-68, pp. 307-330.

12. Allen, C. W., Townsend, D. P., and Zaretsky, E. V., "New Generalized Rheological Model for Lubrication of a Ball Spinning in a Nonconforming Groove. NASA TN D-7280, 1973.

13. Townsend, D. P., Allen, C. W., and Zaretsky, E. V., "Friction Losses in a Lubricated Thrust Loaded Cageless Angular Contact Bearing," Proposed NASA Technical Note, 1973.

14. Wolveridge, P. E., Baglin, K. P., and Archard, J. F., "The Starved Lubrication of Cylinders in Line Contact," Proc. Inst. Mech. Engrs. 1970-71, Vol. 185, 81/71, p. D428.

15. Eskinazi, Salamon," Principles of Fluid Mechanics" Allyn and Bacon, Boston, 1968, p. 438.

16. Drutowski, R. C., "Energy Losses of Balls Rolling on Plates," J. Basic Engr., Vol. 81, No. 1, June 1959, pp. 233-239.

17. Dawson, D., and Higginson, G. R., Elastohydrodynamic Lubrication, Pergamon Press (1966).

TABLE 1. - TEST BEARING SPECIFICATIONS

	Type A	Type B
Inside diameter, mm (in.)	20	(0.7874)
Outside diameter, mm (in.)	47	(1.8504)
Width, mm (in.)	14	(0.5512)
Pitch diameter, mm (in.)	33.5	(1.319)
Nominal contact angle, percent	26	17
Inner race curvature, percent	52	53
Outer race curvature, percent	52	54
Number of balls		3
Ball diameter, mm (in.)		7.15 (0.281)
Rockwell C hardness - inner race		62-64
Rockwell C hardness - outer race		62-64
Rockwell hardness - balls		62-64
Surface finish, rms - races, μm (μin.)		0.15 (6)
Surface finish, rms - balls, μm (μin.)		0.025 - 0.05 (1 - 2)

TABLE 2. - CALCULATED VALUES OF FLUID-DYNAMIC DRAG BASED UPON COMPLETELY FILLING AN ANNULAR BEARING CAVITY WITH A HOMOGENEOUS FLUID

[Bearing bore, 20 mm; number of balls: 3, cage, none; temperature, room ambient.]

Fluid	Shaft speed, rpm	Ball orbital speed, m/sec (in./sec)	Reynolds number	Drag coefficient, C_D	Drag force per ball, newtons (lb)	Total drag torque, N-m (lb-in.)
Air	1000	0.7 (27.5)	327	0.55	6.2×10^{-6} (1.4×10^{-6})	0.32×10^{-6} (2.8×10^{-6})
	3000	2.1 (84)	990	0.42	44.5×10^{-6} (10.0×10^{-6})	2.3×10^{-6} (20×10^{-6})
Di-2-ethylhexyl sebacate	1000	0.7 (27.5)	287	0.7	6.2×10^{-3} (1.4×10^{-3})	0.32×10^{-3} (2.8×10^{-3})
	3000	2.1 (84)	880	0.45	35.6×10^{-3} (8.0×10^{-3})	1.8×10^{-3} (16×10^{-3})
Synthetic paraffinic oil	1000	0.7 (27.5)	10.7	4	35.6×10^{-3} (8.0×10^{-3})	1.8×10^{-3} (16×10^{-3})
	3000	2.1 (84)	33	2	169×10^{-3} (38.0×10^{-3})	8.6×10^{-3} (76×10^{-3})

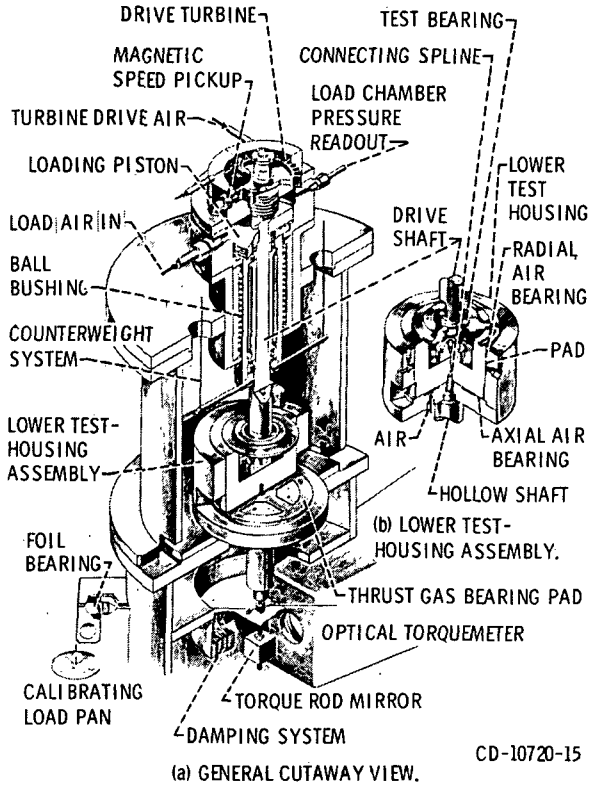

Figure 1. - Bearing torque apparatus.

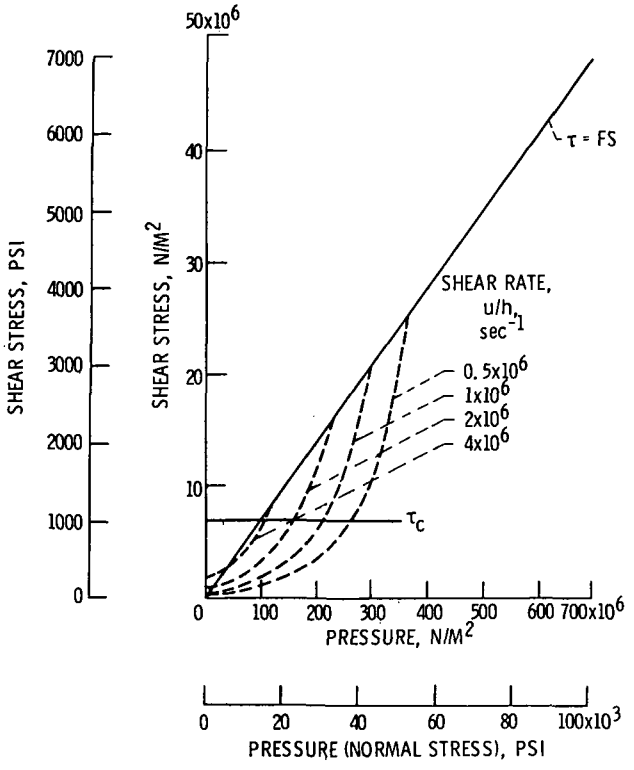

Figure 2. - Shear stress plotted against pressure for synthetic paraffinic lubricant at various shear rates.

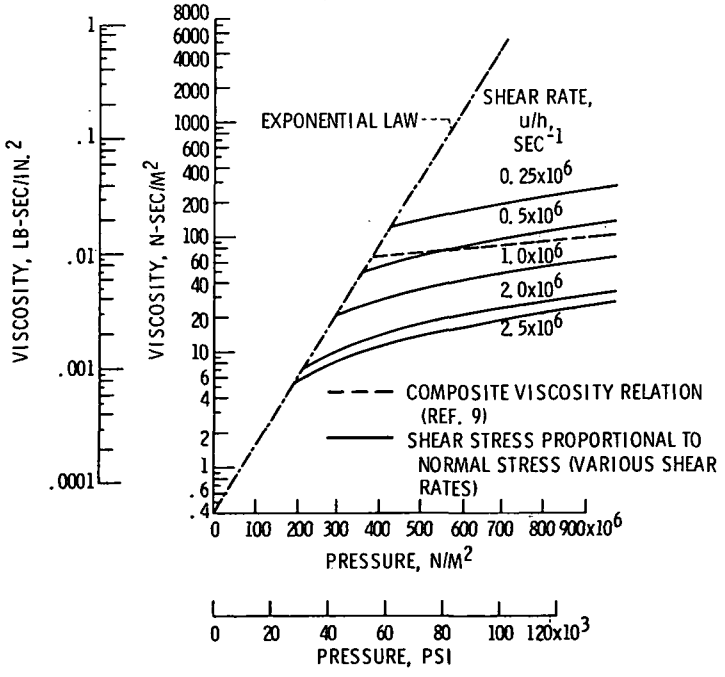

Figure 3. - Equivalent viscosity versus pressure using new rheological model for a synthetic paraffinic lubricant at various shear rates.

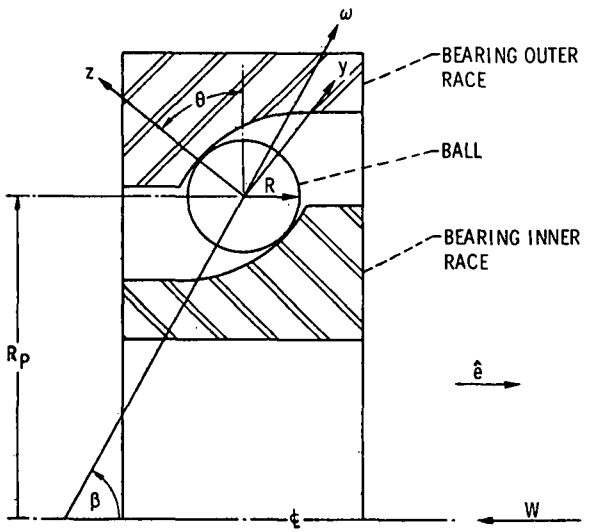

(a) SCHEMATIC OF BALL BEARING.

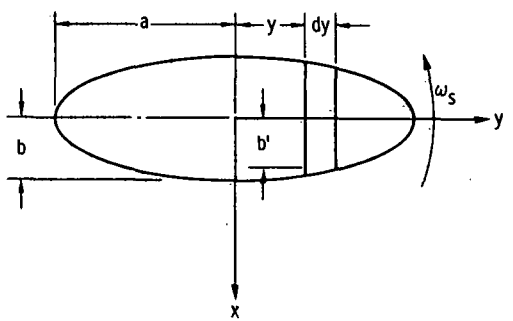

(b) CONTACT ELLIPSE BETWEEN BALL AND RACE.

Figure 4. - Coordinate system used in kinematic analysis of ball bearing.

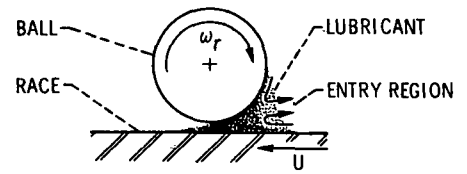

(a) REVERSE FLOW OF LUBRICANT IN ENTRY REGION.

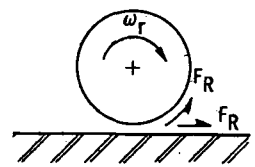

(b) FRICTION FORCES ON BALL AND RACE DUE TO REVERSE FLOW.

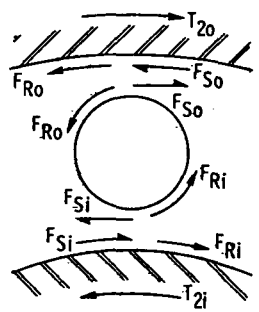

(c) BALL AND RACES SHOWING ALL FORCES NECESSARY FOR EQUILIBRIUM.

Figure 5. - Origin of rolling resistance of ball and race.

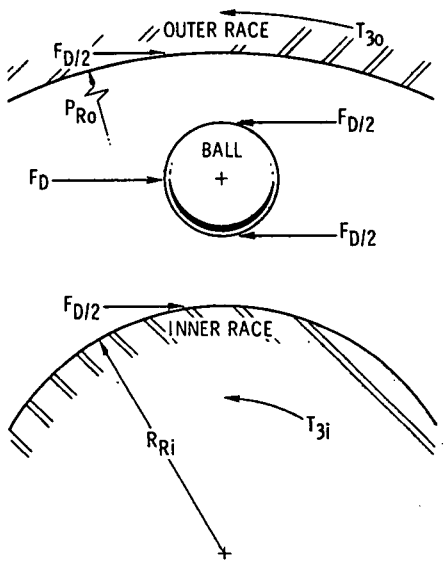

Figure 6. - Fluid-dynamic drag on ball and resulting drag forces on races.

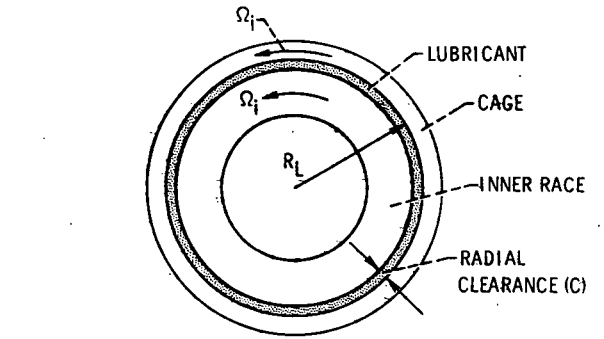

(a) SCHEMATIC OF INNER RACE AND CAGE.

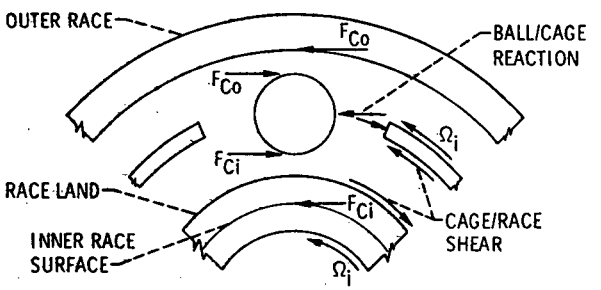

(b) FORCE DIAGRAM.

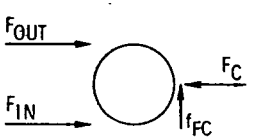

(c) OUTER RACE FORCE DIAGRAM DUE TO CAGE FRICTION.

Figure 7. - Cage drag effects.

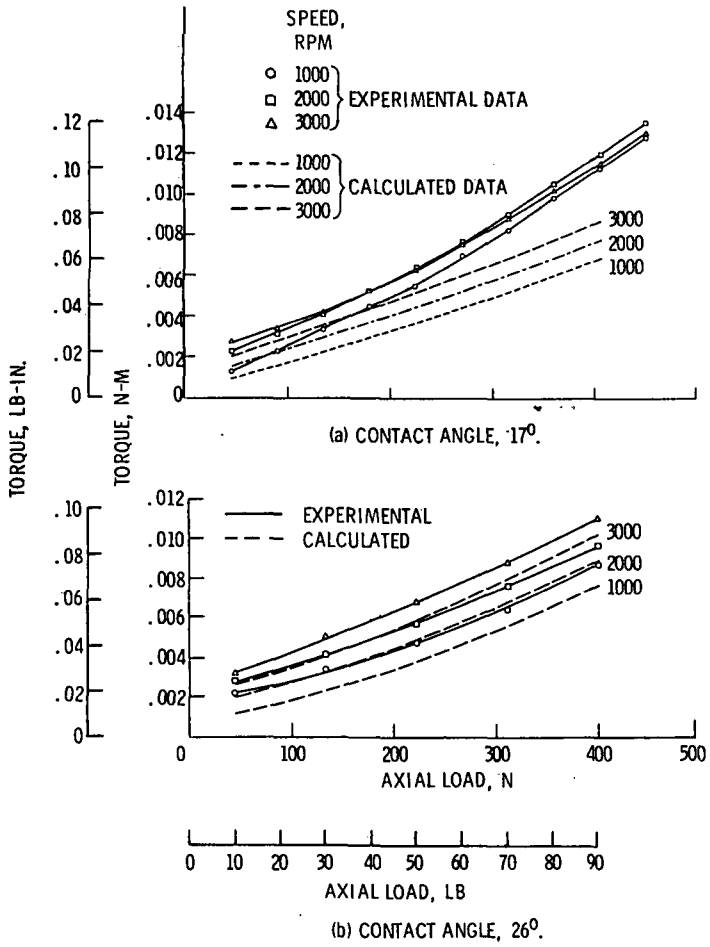

Figure 8. - Comparison of experimental and calculated bearing torque as a function of load for a Di-2-ethylhexyl sebacate lubricant. Bearing bore size, 20 mm; speed, 1000, 2000, and 3000 rpm; number of balls, 3; cage, none; temperature, room ambient; type of lubrication, thin film and oil jet.

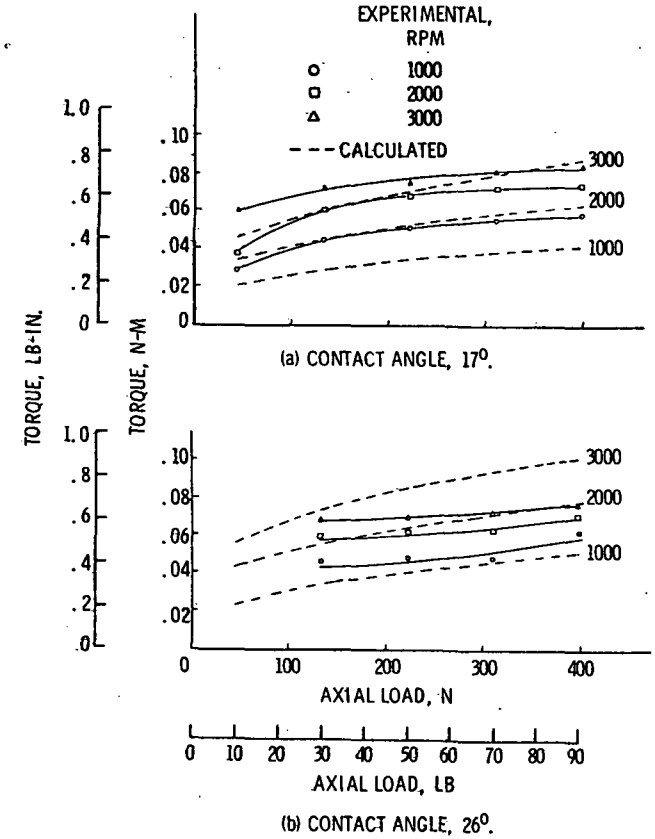

Figure 9. - Comparison of calculated and experimental bearing torque as a function of load for a synthetic paraffinic oil. Bearing bore size, 20 mm; speed, 1000, 2000, and 3000 rpm; number of balls, 3; cage, none; temperature, room ambient; type of lubrication, oil jet.

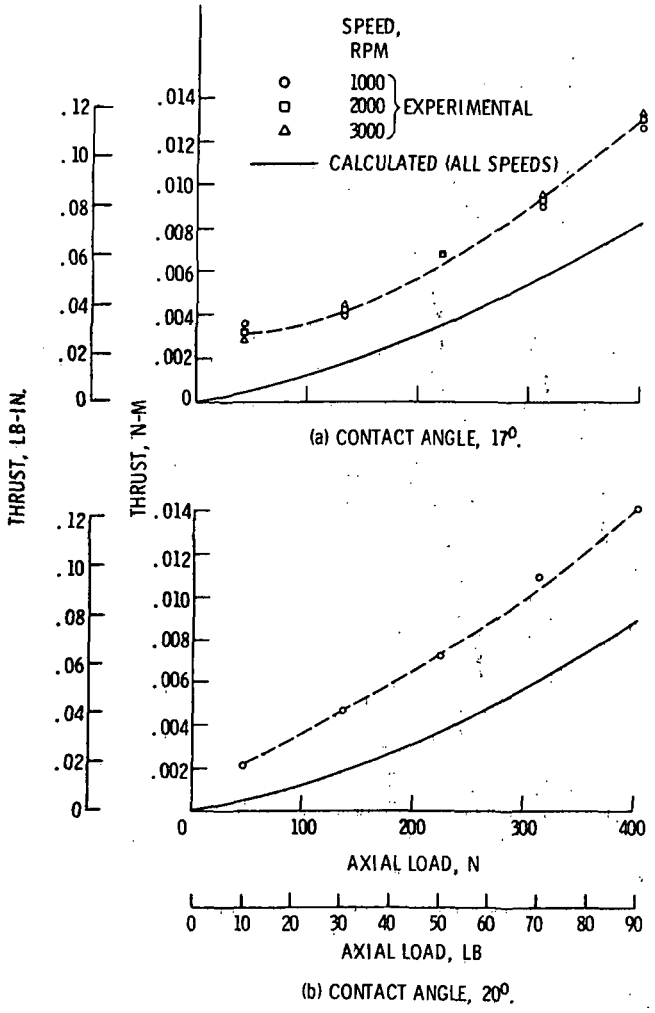

Figure 10. - Comparison of experimental and calculated bearing torque as a function of load for a synthetic paraffinic oil. Bearing bore size, 20 mm; speed, 1000, 2000, and 3000 rpm; number of balls, 3; cage, none; temperature, room ambient; type of lubrication, thin film.

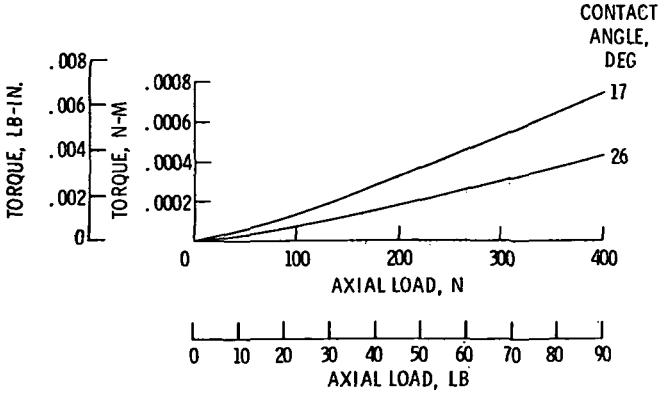

Figure 11. - Calculated bearing torque due to hysteresis as a function of load. Bearing bore size, 20 mm; number of balls, 3; cage, none; lubrication, none.

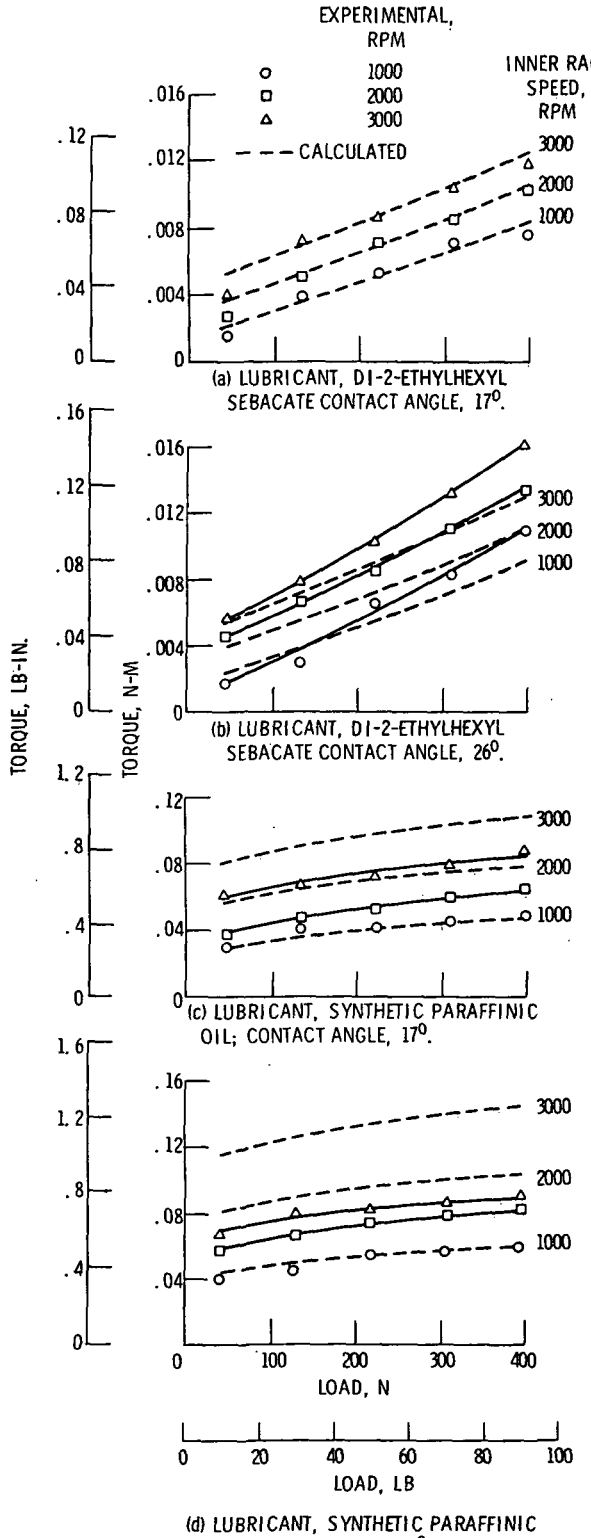

Figure 12. - Comparison of calculated and experimental bearing torque as a function of load for a bearing with an inner-land riding cage; bearing bore size, 20 mm; speed, 1000, 2000, and 3000 rpm; number of balls, 3; temperature, room ambient; type of lubrication, oil jet.

E-7484

NASA-Lewis